REACTIVE TRANSPORT MODELLING OF INJECTION FLUID- RESERVOIR ROCK INTERACTION

Charis Wong[1], Etienne Buscarlet[1], Simon Addison[1], Morgane Le Brun[1]

[1] Mercury NZ Limited, PO Box 245, Rotorua 3040, New Zealand

Charis.Wong@mercury.co.nz

Keywords: *injectivity, injection well, amorphous silica deposition, geochemical modelling, fluid rock interaction*

ABSTRACT

One-dimensional radial reactive transport TOUGHREACT models have been created for three injection wells as part of the injection management strategy in an operating geothermal field. This provides an understanding of the injection fluid-reservoir rock interaction which shapes the behavior and characteristics of the injection wells. Three main factors that contribute to the injection well behavior are identified including feedzone thickness, injection flow rate and variations, and fracture porosity-permeability relationship of the geologic media injected into.

This paper also discusses the potential opportunities in injection management such as injection configuration, brine-condensate switching and new well acidising. It demonstrates the use of geochemical modelling as a tool to assist in optimizing the injection strategy for reservoir management.

1. INTRODUCTION

As part of the injection management strategy in an operating geothermal field, reactive transport models have been created to understand the injection fluid-reservoir rock interaction which impacts the injection well behavior and characteristics. This study has been conducted based on three injection wells representing test cases for early and later stages of injection operation, different feedzone thickness, variation in injection flow rate due to operational purposes and the fracture porosity-permeability relationship of the geologic media that has been injected into.

1.1 Conceptual Model of reservoir process

Sulfuric acid dosing takes place at the station to mitigate silica scaling risk. As a result of this operational procedure, the flashed injection brine is predominantly low in pH and high in silica and sulfate. The purpose of these models is to simulate the interaction between injection fluid and reservoir rock.

With the nature of this injection fluid, the fluid-rock interactions considered are listed as follows:

a) Amorphous silica deposition due to the oversaturated silica content after flashing at the plant.

b) Calcite dissolution in rock fractures due to low temperature and acidic nature of the injection fluid over time.

c) Anhydrite deposition due to the high sulfate content as a result of sulfuric acid dosing at the plant.

d) Bulk rock dissolution (in matrix) due to the acidic nature of fluid over time.

1.2 Flow model set up

Reactive transport models are created with the use of TOUGHREACT (Xu et al, 2012) and EOS1 as the equation of state. The models are one-dimensional and liquid only. The 100 radial grid blocks are built to extend logarithmically up to 1000m with the first block diameter as 0.2m wide (Figure 1). The logarithmic increments allow capturing near wellbore condition in a finer scale. The height of the grid blocks is dependent on the total thickness of well feedzones. This allows consideration of all the feedzone distribution in a wellbore.

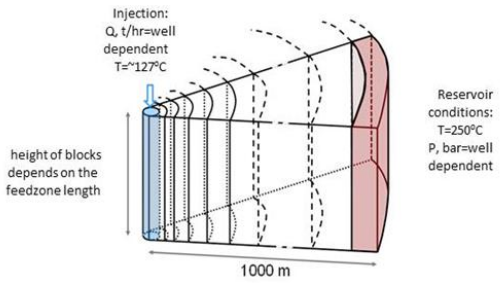

Figure 1: Schematic diagram of model set up

A MINC approach is chosen (two domains: fracture and matrix). Physical parameters such as matrix permeability, fracture and matrix porosity and volume percentage are derived from the full field consent numerical model to ensure consistency (Table 1). Fracture spacing of 150m wide has been used.

Table 1: MINC model properties

MINC model properties	Fracture	Matrix
Fracture Spacing (m)	150	-
Permeability (m^2)	varies with wells	5E-17
Porosity (%)	90	10
Volume (%)	0.95	99.05

To check that the height of the block and the fracture permeability used in the model are representative of the field, the transmissivity was calculated for each well and compare to the field values obtained with interference tests. The values range between 40 D.m and 100 D.m, which is representative of the field. Input reservoir pressure is dependent on specific wells (Table 2). It is calculated using the pressure at the pivot point from the last pressure temperature survey (PTS) and applying the field pressure gradient to obtain the pressure at the centre of the block of the model. Injection fluid temperature is continuously measured on the injection line.

Reactive transport models have been set up for three injection wells (hereafter referred to as well A, well B and well C) of different characteristics, their modelled feedzone

thicknesses and injected flow rate range are summarised in Table 3.

Table 2: Modelled reservoir pressure and temperature

Model	Pressure (bar)	Temperature (°C)	Silica (mg/kg)
Reservoir condition	well dependent	250	680
Injection fluid*	-	127	820
* Injection fluid temperature input data corresponds to measured time series			

Table 3: Modelled well characteristics

	Well A	Well B	Well C
Modelled feed zone thickness (m)	670	430	130
Flow rate range (t/hr)	600	800 (initial), 400 (late)	450
Injection history	Early stage	Late stage	Late stage

1.3 Geochemical parameters

1.3.1 Mineralogy of reservoir rock

Mineralogy of the rock mass is estimated based on drill core in greywacke where all the injection feedzones are located. Illite, clinozoisite and clinochlore are used in the model, which are equivalent to clay, epidote and chlorite in the Lawrence Livermore National Laboratory thermodynamic database (Wolery et al, 1992) (Table 4**)**. Initial reactive surface areas are referenced in Xu et al. (2006), while kinetic rate constant and activation energy are extracted from Palandri and Kharaka (2004). Amorphous silica is the only mineral that has both dissolution and precipitation kinetic rates available, while other minerals' kinetic rates are predominantly based on dissolution kinetic rate. The kinetic rates are independent of the pH.

Table 4: Modelled mineralogy and associated kinetic parameters

Mineral present in Well A drillcore Greywacke feedzone area	Equivalent name in LLNL database	Initial volume fraction	Initial reactive specific surface area (cm^2/g)	Kinetic rate constant at 25°C ($mol/m^2/s$)	Activation energy (kJ/mol)
Clay	illite	0.13	151.6	1.0E-13	62.8
Chlorite	clinochlore	0.13	9.8	3.0E-13	88.0
Calcite	calcite	0.19	9.8	1.5E-06	23.5
Quartz	quartz	0.13	9.8	4.0E-14	90.9
Epidote	clinozoisite	0.19	21.0	1.0E-12	70.7
anhydrite	anhydrite	nil	9.8	6.5E-04	14.3
Amorphous silica (dissolution)	Silica Amorphous	nil	variable	4.9E-13	76.0
Amorphous silica (precipitation)				3.8E-10	49.8

1.3.2 Aqueous geochemistry

The reservoir fluid chemistry has been chosen so as to be representative of the natural reservoir fluid condition. Separated brine and gas has been recombined as single phase through geochemical modelling software WATCH 2.4 (ISOR, 2013) which has been integrated into the WATCH Automator by Zeng (2013). The chemical parameters considered in this model include H^+, Na^+, K^+, Ca^{2+}, Mg^{2+}, Al^{3+}, HCO_3^- and SiO_2. Carbon dioxide gas content is represented in the form of bicarbonate in the TOUGHREACT chemical input. The model input silica content of the flashed injection brine at ~127°C is 820mg/kg, while the silica content under reservoir condition is 680mg/kg.

1.3.3 Reaction rate

The dissolution-precipitation reaction modelled is a surface controlled reaction, and the same methodology as Xu et al. (2012) and Buscarlet and Hernandez (2014) has been adopted in this paper. Majority of the mineral reactions are based on the following equation (referenced from TOUGHREACT manual, Xu et al, 2012):

Equation 1

$$r = k_{25^oC} exp\left[\frac{-E_a}{R}\left(\frac{1}{T}-\frac{1}{298.15}\right) A\left[1-\left(\frac{Q}{K}\right)\right]\right]$$

The first part of the equation approximates the rate constant as a function of temperature as rate constants are generally reported at 25°C. From the equation, r ($mol.m^{-2}.s^{-1}$) is the rate of dissolution/precipitation k_{25^oC} ($mol.m^{-2}.s^{-1}$) as the dissolution or precipitation kinetic rate constant at 25°C, E_a ($kJ.mol^{-1}$) is the activation energy, R as gas constant (8.314 $J.K^{-1}.mol^{-1}$), T (K) as absolute temperature, A (m^2/kg_{H2O}) as the specific reactive surface area, Q as the activity product for the reaction and K as the equilibrium constant of the reaction. There is generally a large variability in the experimental reaction constant k_{25} and specific reactive surface area A, and discrepancies are also commonly observed between field and experimental values.

Carrol et al. (1998) has conducted a study on amorphous silica precipitation behavior comparing laboratory experiments and field experiments based on the Wairakei geothermal field. The study shows that amorphous silica precipitation rates in geothermal field is about three orders of magnitude higher than theoretical amorphous silica precipitation rates. Therefore a modified kinetic rate equation is utilized for amorphous silica as follows:

Equation 2

$$r = k_{25^oC} exp\left[\frac{-E_a}{R}\left(\frac{1}{T}-\frac{1}{298.15}\right) A\left[\left(\frac{Q}{K}\right)^{4.4}-\frac{1}{\left(\frac{Q}{K}\right)^{8.8}}\right]\right]$$

2. MODEL RESULTS

2.1 Modelled versus observed injectivity index

Model matches have been achieved between observed and modelled injectivity indices (Figure 2). The modelled injectivity index is defined by the following equation:

Equation 3

$$II = \frac{\boldsymbol{Flow\ rate}}{\boldsymbol{P_b - P_i}}$$

Where flow rate (t/hr) is based on the flow rate of the first block which has been set up to represents the wellbore condition. P_b(bar) is the pressure of the first block (representing the wellbore pressure) and P_i(bar) is the initial reservoir pressure. The observed II is defined by the same ratio, the wellbore pressure being calculated using assumptions on friction factors, the reservoir pressure being constant over time.

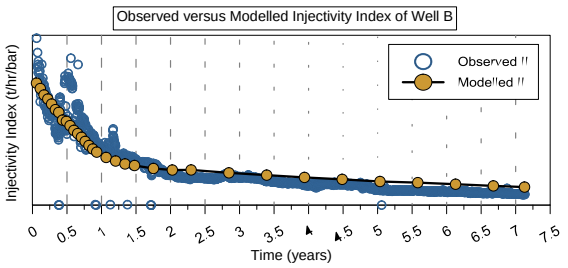

Figure 2: Well B Observed and modelled injectivity index

Model matches are achieved by adjustment of the two main controlling parameters, consisting the reactive surface area and the permeability law. The change in porosity is associated to the volume change as a result of mineral dissolution/precipitation, which in turn alters the permeability based upon the porosity-permeability relationship. Two main permeability laws have been tested in the model matches including the cubic law (Equation 4) and the Verma-Pruess law (Equation 5), with varying critical porosity and power exponent.

Equation 4

$$k = k_i \left(\frac{\emptyset}{\emptyset_i}\right)^3$$

Where k is the permeability (m^2), k_i the initial permeability (m^2) and $\emptyset_i$ is initial porosity. Well A and Well C can only be matched with the use of the Verma-Pruess law where the critical porosity remains at 0.15 and 0.20 with power exponent of 0.9 and 1.9 respectively. The Verma-Pruess law considers a more complex porosity-permeability relationship of geologic media such as pore size distribution, pore shapes etc (Verma and Pruess 1988 from TOUGHREACT MANUAL, Xu et al 2012).

Equation 5

$$\frac{k}{k_i} = \left(\frac{\emptyset - \emptyset_c}{\emptyset_i - \emptyset_c}\right)^n$$

Where $\emptyset_c$ is the critical porosity and n is a power exponent. The Verma-Pruess law does not only consider the porosity reduction but also the pore space connectivity. For example, precipitation at a pore throat can lead to the disconnection of the pore space, reducing the overall permeability, indicating strong dependence of permeability on variation in porosity.

Modelling results for Well A are shown in Figure 3. Table 5 outlines the permeability parameters for the closest matches of each individual reactive surface area. It can be noted that the critical porosity remains closely between 0.15 to 0.2.

Model matches are mostly achieved with larger initial reactive surface area for amorphous silica, while the smaller surface area generally shows a smaller decline. Well A in Figure 3 also shows a smaller decline for smaller surface area, while three model matches can be achieved for larger surface area. Well A is the only well with three possible solutions, while only one unique solution can be achieved by Well B and Well C.

Sensitivity analysis has also been conducted to compare fracture spacing of 150m and 50m. No major difference can be observed between the modelled injectivity indices. However a more comprehensive test should be conducted for this investigation.

Table 5: Well A initial reactive surface area and permeability law parameters

Label on the graph	Initial reactive surface area (cm^2/g)	References	Well A Cubic law and Verma-Pruess law	
			Critical porosity	Power exponent
			$\emptyset_c$	n
A	$1.0x10^7$	Xu et al. 2012	Cubic Law	
B	$1.0x10^1$	Xu et al. 2012	0.2	0.5
C	$1.0x10^3$	Bethke 2011	0.2	2
D	$2.0x10^4$	Bethke 2011	0.15	0.9
E	$1.0x10^7$ (initial model)	Xu et al. 2012	0.2	0.8
F	$4.8x10^9$	Xu et al. 2012	0.2	1.4

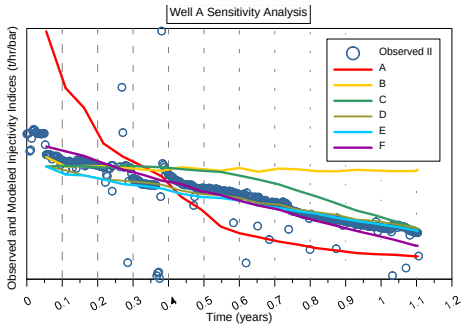

Figure 3: Well A sensitivity analysis of reactive surface area and permeability laws.

2.2 Injection fluid-reservoir rock interaction

Upon injection, a gradual reduction in fracture porosity is modelled in all the wells (Figure 4). After circa 1 year of injection, Well A shows a more intense and more localized reduction in porosity, within the first 20 m from the wellbore. In comparison, for the same time of injection, Well C shows a less intense and more widespread porosity reduction of up to 100 m from the wellbore. A larger porosity reduction within immediate distance of the wellbore is reached by Well A over a much shorter period of time than well C. Fracture permeability is also reduced subsequently to the porosity reduction (Figure 5). Note that Well A and Well C have different starting fracture permeability.

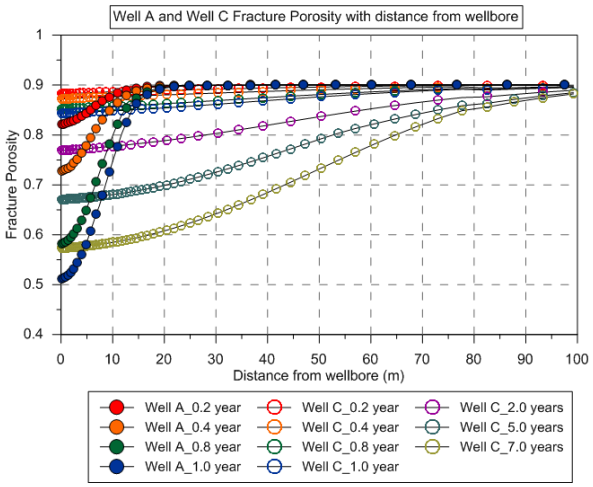

Figure 4: Fracture porosity for Well A and Well C over time

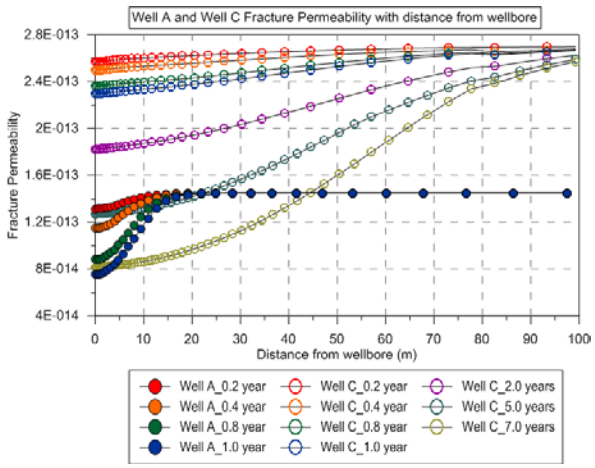

Figure 5: Fracture permeability for Well A and Well C over time

The change in porosity and permeability is resulting from the injection fluid-reservoir rock interaction (Figure 6). The quantity of minerals is reported as a change in abundance (tons per m^3 fracture dissolved or precipitated) in this paper. Upon injection, amorphous silica is deposited from silica supersaturated brine. Amorphous silica deposition is the main contributor to the porosity-permeability reduction with its quantity being an order of magnitude higher than other minerals (Figure 6). Illite is another mineral that has been deposited as a result of acidized brine injection. However, only a very small amount of illite is deposited in contrast to silica, and is not a major contributor to the permeability reduction.

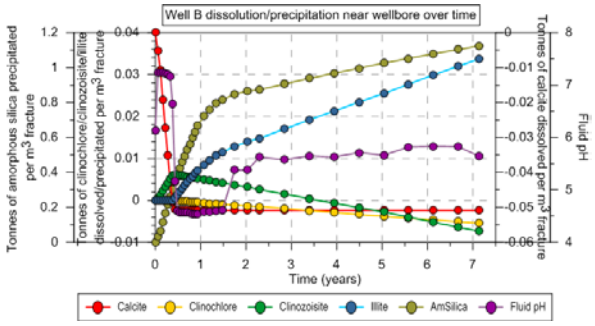

Figure 6: Well B mineral dissolution/precipitation near wellbore over time

2.2.1 Amorphous silica deposition

pH modification is carried out through the addition of sulfuric acid at the station to inhibit amorphous silica polymerisation. The inhibition property of the acid dosing cannot be simulated in this model. Experimentally, a delayed deposition is observed as a result of inhibited polymerisation. Gallup (1997) showed that sulfuric acid inhibits silica scaling by retarding the kinetics of silica polymerisation and by promoting silica solubility by forming complexes with silicic acid. Studies conducted by Brown (2011) and Addison et al. (2015) also showed a decrease rate of colloid formation at lower pH, which assists in delaying polymerisation for hours. In absence of reservoir fluid neutralisation, the silica inhibition should be effective near wellbore in the reservoir.

Well A shows a localized deposition of up to 0.9 tons per m^3 fracture within 20 m from the wellbore after 1.1 years of injection; while Well C shows a deposition of only up to 0.2 tons per m^3 fracture within 100 m from the wellbore after 1.5 years of injection (Figure 7). A more widespread deposition is observed for Well C with lower injection load and smaller feedzone thickness than Well A with higher injection load and larger feedzone thickness. The deposition behavior shows a competition between injection flow rate and feedzone thickness.

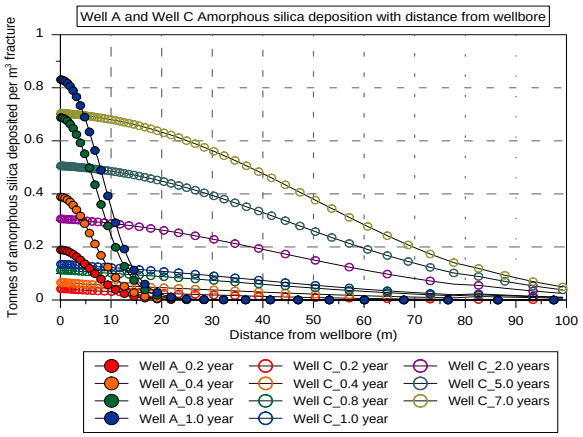

Figure 7: Amorphous silica deposition for Well A and Well C

2.2.2 Calcite dissolution and fluid pH neutralisation during early stage of operation

Due to the low temperature and acidic nature of the injection brine, substantial amount of calcite is dissolved. The calcite dissolution shows a similar spatial distribution to the silica deposition. The smaller feedzone thickness and lower injection load, the more widespread and less intense the calcite dissolution is observed and vice-versa (Figure 8).

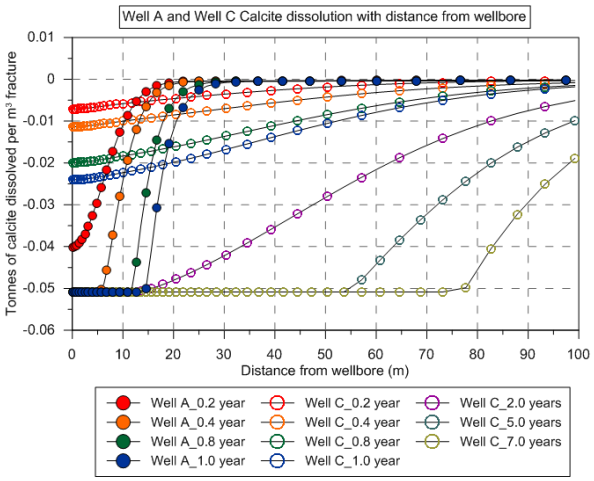

Figure 8: Calcite dissolution for Well A and Well B

As a result of calcite dissolution by reacting with the acidic injection brine, the reservoir fluid pH is neutralised and calcium ions are released into the reservoir fluid (Figure 9, Figure 10) as described by the following reaction:

Equation 6

$$H^+ + CaCO_3 \rightarrow Ca^{2+} + HCO_3^-$$

As the calcite dissolution process reaches further away from the wellbore, a similar calcium and pH neutralisation front is modelled. Well A reaches complete calcite dissolution by 0.4 year, while Well C took about 2 years to reach complete

dissolution. This trend is also observed in the aqueous calcium and fluid pH behavior over time.

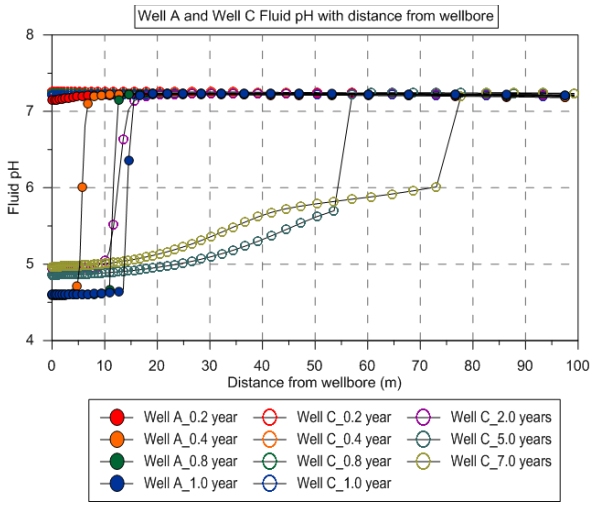

Figure 9: Fluid pH for Well A and Well C

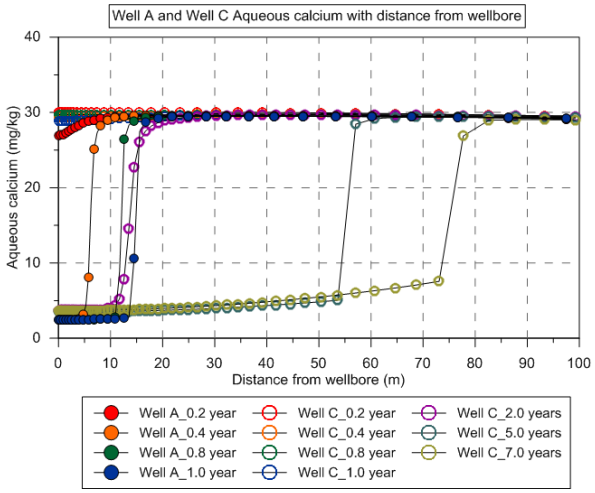

Figure 10: Aqueous calcium for Well A and Well C

2.2.3 Anhydrite deposition potential

Due to sulfuric acid dosing contributing aqueous sulfate to the injection fluid, the anhydrite scaling risk in the reservoir has also been assessed. No anhydrite deposition is observed within the close vicinity to the wellbore. Anhydrite saturation indices remain below saturation limit over time for Well A and Well C (Figure 11). It can be noted that the increase in anhydrite saturation indices corresponds to the increase in calcium in solution, following in turn the calcite dissolution front (Figure 10).

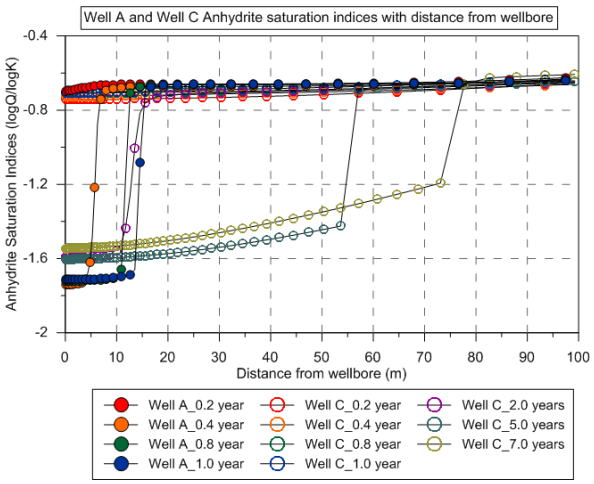

Figure 11: Anhydrite saturation indices for Well A and Well C

2.2.4 Bulk rock dissolution and pH neutralisation during late stage of operation

Well A represents an early stage of the well operation (1.1years) while Well C represents a later stage (7.5years). During the early injection history, a sharp pH neutralisation front is resulting from the fast dissolution kinetics of calcite (Figure 9).

At a later stage of operation, despite complete calcite dissolution being achieved, gradual pH neutralisation is modelled, trending away from the wellbore with distance. This is due to the bulk reservoir rock acid dissolution with mineral such as clinochlore (chlorite) and clinozoisite (epidote), as described by the following reactions:

Equation 7 *Clinochlore*

$$16H^+ + Mg_5Al_2Si_3O_{10}(OH)_8 \rightarrow 5Mg^{2+} + 2Al^{3+} + 3SiO_2 + 12H_2O$$

Equation 8 *Clinozoisite*

$$13H^+ + Ca_2Al_3Si_3O_{12}(OH) \rightarrow 2Ca^{2+} + 3Al^{3+} + 3SiO_2 + 7H_2O$$

These reactions have much slower dissolution kinetic rates than calcite (Figure 12, Figure 13). This neutralisation effect is mostly apparent further away from the wellbore, while closer to the injection well the reservoir fluid pH remains similar to the injection fluid pH.

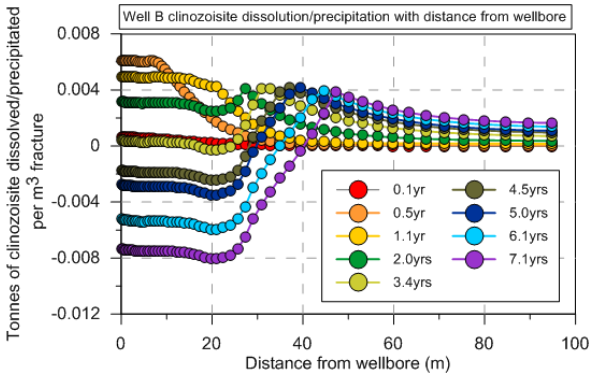

Figure 12: Well B clinozoisite dissolution/precipitation

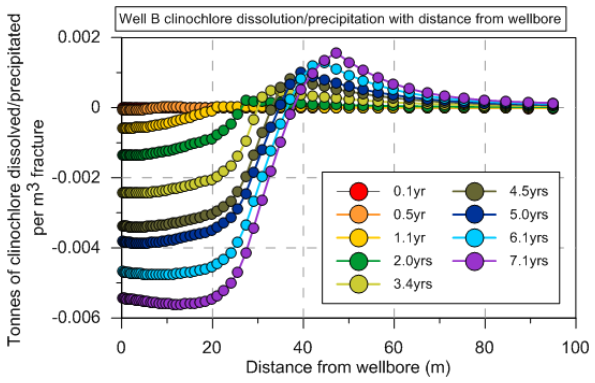

Figure 13: Well B clinochlore dissolution/precipitation

3. DISCUSSION

3.1 Controlling factors

Given the different characteristics modelled for each individual wells, three controlling factors have been identified that influence the behavior of injection fluid-reservoir rock interactions.

3.1.1 Porosity-permeability relationship of the geologic media

Figure 14 represents the fracture porosity-permeability relationship of the geologic media used in the model for Well A, Well B and Well C to match the observed injectivity index accordingly.

Assuming the same injection flow rate and the same feedzone geometry for each well, Well A shows a minimal fracture permeability impact with the same amount of fracture porosity reduction relative to Well B and Well C. It follows that for the same amount of silica deposited in each well (i.e. same reduction in fracture porosity), there will be less impact on fracture permeability in Well A.

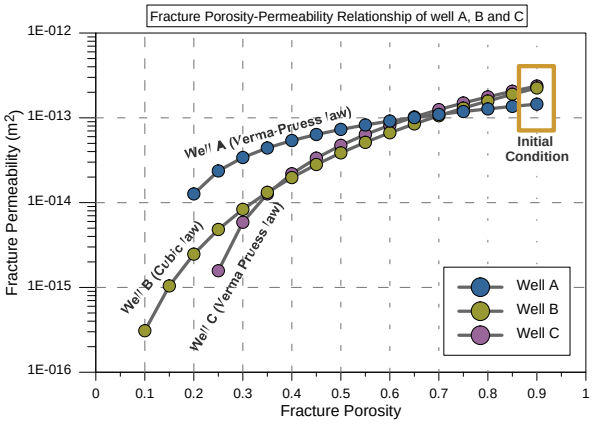

Figure 14: Fracture porosity-permeability relationship of Well A, Well B and Well C

3.1.2 Feedzone thickness

Assuming the same injection flow rate, model results show that the reservoir rocks reactions with the injection fluid will take place further away from the wellbore in injection wells with smaller feedzone thickness compared to wells with larger feedzones thicknesses (Figure 15). As a result, amorphous silica deposition is localized within the close vicinity of the wellbore for wells with larger feedzone thickness; whereas it is more widespread further away from the wellbore for wells with thinner feedzone thickness.

This can be illustrated through Figure 16 with Well A and Well B amorphous silica deposition at same injection flow rate of 684t/hr. It shows that deposition is more localized up to 20m from wellbore; whereas deposition is slightly more widespread for Well B of up to 40m from wellbore.

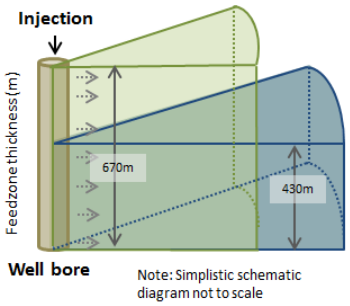

Figure 15: Schematic diagram of wells with different feedzone thickness

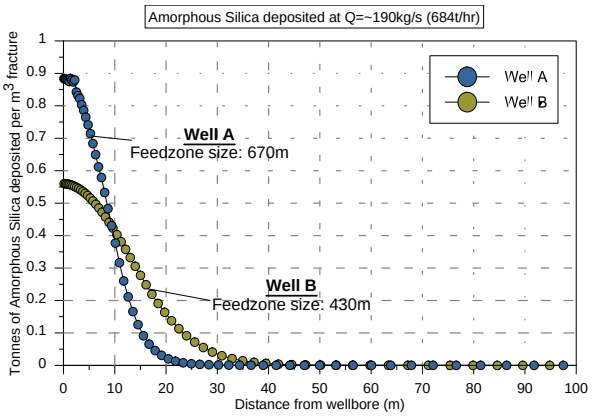

Figure 16: Amorphous silica deposition for Well A and Well B at injection load of 684t/hr

3.1.3 Injection flow rate – quantity and extent of deposition

Modelling results (Figure 17) show more amorphous silica is deposited in Well A compared to Well B and Well C after 1 year of injection. Despite a higher injection flow rate at Well B during the first year of operation, it has deposited less amorphous silica at immediate vicinity of the wellbore than Well A. This can potentially be due to the larger feedzone thickness where amorphous silica is more localized at near well bore of Well A, while a more wide spread deposition is observed for Well B. Well C shows the least amount of amorphous silica deposited near the injection wellbore and more widespread up to 100m further away from the wellbore.

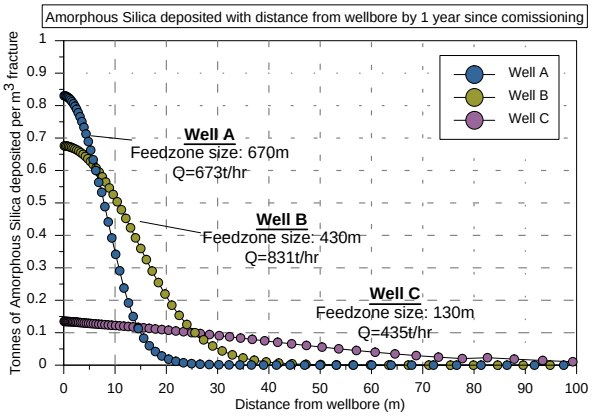

Figure 17: Amorphous silica deposition after 1 year of injection since commissioning for Well A, Well B and Well C

The increasing amount of amorphous silica deposition appears to be related with the maximization of the injection flow rate. This is due to the higher quantity of aqueous silica introduced to the reservoir, made available for deposition (Figure 18). A steeper increase in amorphous silica deposition is observed during periods of high injection flow rate, while a smaller increase in deposition is modelled for average injection flow (~450t/hr).

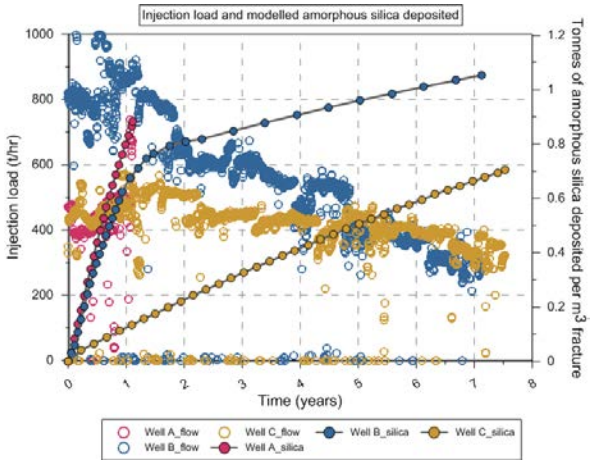

Figure 18: Measured injection load and modelled amorphous silica deposition

Figure 19 also illustrates the correlation between amorphous silica deposition and the fracture porosity reduction. At an early stage of injection, where the flow rate is maximized, Well A and B share a similar magnitude of porosity reduction by 28 to 38% respectively. Later on, when the injection load is reduced from ~800t/hr to ~400t/hr, a more gradual decline in porosity by 2.5% is modelled in Well B. A similar magnitude of porosity reduction is modelled in Well C under a similar injection flow rate.

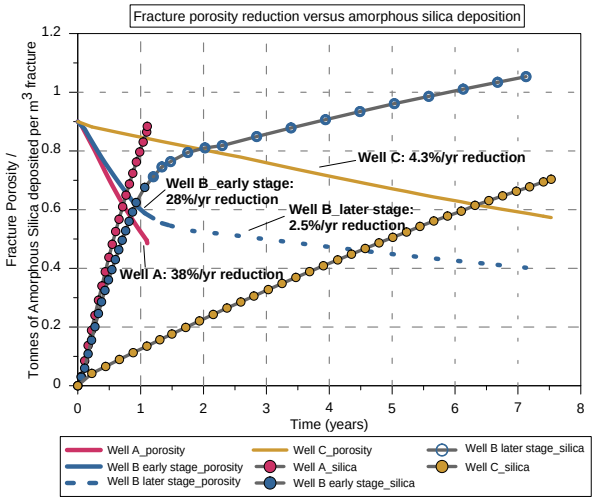

Figure 19: Fracture porosity reduction versus amorphous silica deposition

3.2 Injection fluid-reservoir rock interactions and pH neutralisation

Modelling results suggest that the overall reservoir pH neutralisation over time is taking place in the vicinity of the injection well as a result of injection fluid-reservoir rock interaction, as summarized by the schematic diagram in Figure 20. During an early stage of operation (A), the injected fluid pH neutralisation front is pushed away from the wellbore. This front is sharp and pronounced as a result of the fast dissolution kinetics of calcite. Fluid remains at injection pH near wellbore. At a later stage of operation (B), calcite is completely dissolved close to the wellbore and bulk rock acid dissolution including minerals such as clinochlore and clinozoisite is initiated, releasing calcium and magnesium to reservoir fluid. Due to the slow dissolution kinetic rate of these silicates, a gradual neutralisation is modelled rather than a sharp front. The quantity of clinochlore and clinozoisite dissolved in the reservoir is an order of magnitude less than calcite, leading to a smaller impact in pH neutralisation comparatively. Another factor that could play a role in influencing the pH neutralisation is the variation in injection flow rate for operation purposes (C). A higher injection flow rate pushes the pH neutralisation front further away from the wellbore due to increased acid dissolution of bulk rock; and contrarily, a lower injection flow rate results in a pH neutralisation front being closer to the wellbore.

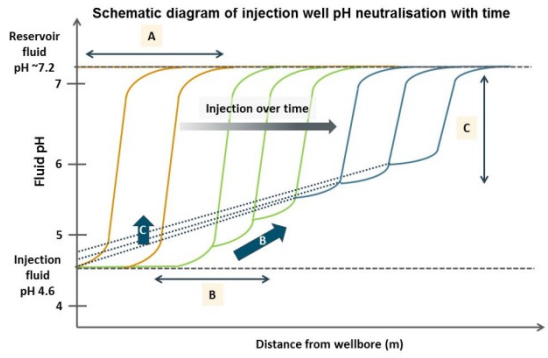

Figure 20: Schematic diagram of injection fluid pH neutralisation with time. A represents early stage of operation, B a later stage of operation, while C refers to a change in injection flow rate due to operation purposes

3.3 Opportunities

Based on the understanding obtained from the modelled injection fluid-reservoir rock interactions, further testing has been conducted to identify opportunities for injection management.

3.3.1 Injection load optimization

A sensitivity analysis has been conducted on the injection flow rate to test the impact on fluid-reservoir rock interaction. For Well C, an increased flow of up to 600t/hr has been modelled to compare with the operational flow (model matched to the observed injectivity indices, average injection rate at ~427t/hr) (Figure 21). Elevated injection flow rate has increased the impact on the well performance due to increased aqueous silica introduced to reservoir available for amorphous silica deposition (Figure 22).

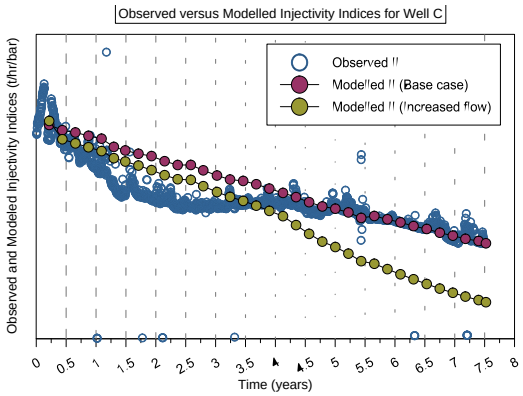

Figure 21: Observed and Modelled injectivity indices for Well C

Despite the increased amorphous silica deposition, the elevated injection flow rate has increased the calcite dissolution, pushing the pH neutralisation front further from wellbore (Figure 22). It suggests that a "maximized injection load" strategy could be beneficial, given a robust pH inhibition system and minimal pH neutralisation in the reservoir is achieved.

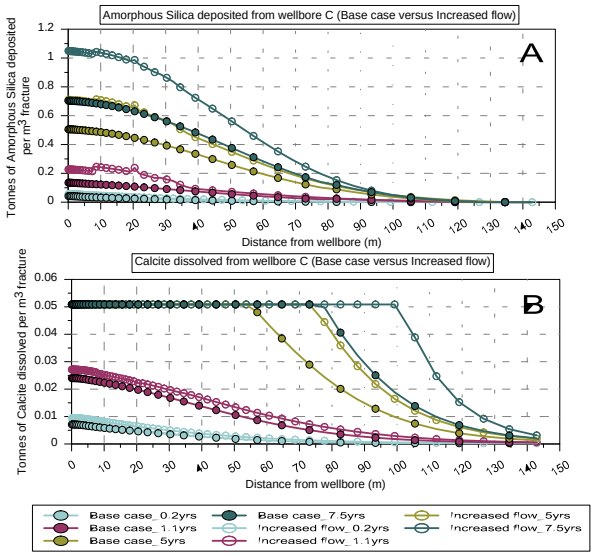

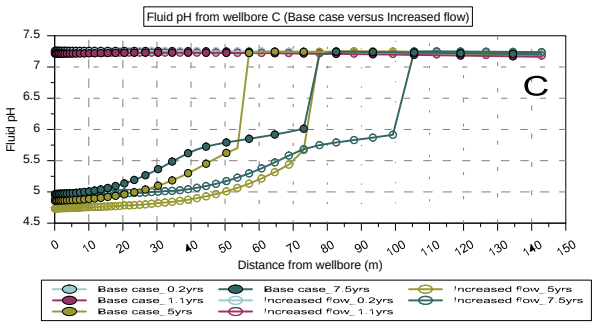

Figure 22: Well C Base case and increased flow scenario. A: Amorphous silica, B: Aqueous calcium, C: fluid pH.

3.3.2 Injection configuration

It has been observed in the field that condensate injection provides some thermal stimulation of injection wells, owing to the low temperature of the injectates. The mechanism of thermal stimulation is based on the opening of fractures as a result of thermal contraction as low temperature fluid is injected into a high temperature reservoir environment (Grant and Bixley 2011). Condensate-brine injection switching shows potential as an injection strategy to gain short term injection capacity. Apart from benefits of thermal stimulation, condensate injection also helps to reduce amorphous silica deposition. Injection condensate contains 0.76mg/kg of aqueous silica as opposed to 817mg/kg of aqueous silica in injection brine. With the injection of a fluid which is under-saturated with respect to amorphous silica, it has the potential to dissolve amorphous silica.

Two scenarios have been conducted for one year of injection in Well A: one with the injection of brine, another one with four phases of condensate-brine switching (Figure 23). This model only accounts for chemical reaction; no mechanical effect of thermal stimulation has been modelled. Figure 23 shows condensate-brine switching has reduced the amount of amorphous silica deposited by 0.1 tons per m^3 fracture compared to brine-only injection. This is due to the amorphous silica dissolution that has taken place during each phase of condensate injection, and the absence of further silica deposition (compared to brine injection). This reduction in amorphous silica deposition is also reflected in the decreased fracture porosity and permeability decline comparable to brine only injection (Figure 24).

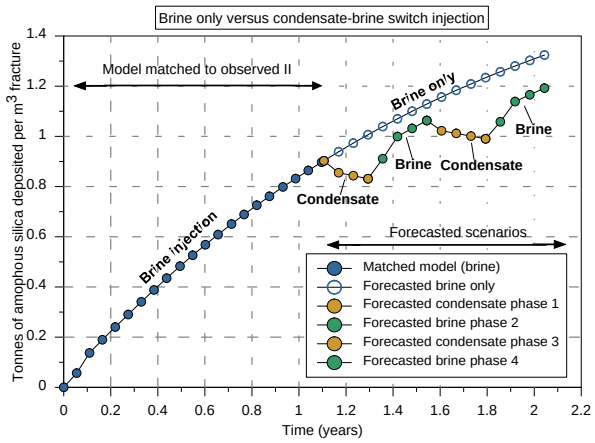

Figure 23: Amorphous silica deposition for brine only injection and condensate-brine switch scenarios (based on Well A)

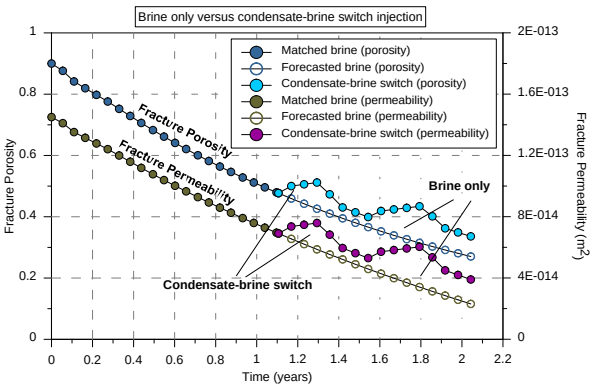

Figure 24: Fracture porosity and permeability for brine only injection and condensate-brine switch scenarios (based on Well A)

3.3.3 New well acidising design

Modelling results suggest that the reservoir fluid pH neutralisation can be caused by calcite dissolution during early stage of operation. This may potentially hinder the silica polymerisation inhibition property from acid-dosing once the injection fluid reaches reservoir. A modelling exercise has been conducted hypothesizing that the removal of calcite in reservoir rock can potentially minimize the pH neutralisation effect during early stage of operation. This modelling exercise simulates the acidising of a newly drilled injection well in order to remove the reservoir calcite close to the injection wellbore. This could hypothetically optimize the acid inhibition properties of the injection brine. The modelling experiment workflow has been summarized in Figure 25. Sequence of condensate injection has been modelled to simulate the chemical effect of the thermal stimulation. The mechanical effect of thermal stimulation cannot be accounted for in this model. Injection of 600m^3 of 10% hydrochloric acid has been modelled to remove calcite around the wellbore in the reservoir. This is followed by condensate injection to simulate routine post-acid flushing procedure to push and dilute any excess acid and aqueous calcium further away from the wellbore. The modelling of brine injection is then carried out. This sequence of models is hereafter referred to as "acidising scenario". It is compared with a model considering direct brine injection with no acidising, hereafter referred to as "direct brine scenario".

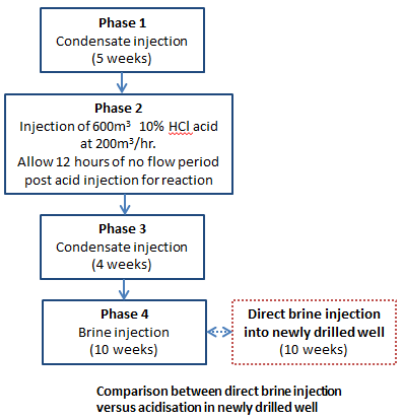

Figure 25: Modelled sequence of acidising at newly drilled well

Calcite dissolution as a result of phase 4 (brine injection stage) is shown in Figure 26. "Acidising scenario" shows complete calcite dissolution within the first 7m from the wellbore as a result of acidising during phase 2. This means a neutralized circular area of up to 154m^2 would have been gained around the wellbore. The acid dosed brine injection during phase 4 leads to further dissolution of calcite between 7 to 20 m over time. A 2% increase in fracture porosity is resulting from this acidising operation. Continuous calcite dissolution is modelled for the "direct brine scenario", and after 10 weeks of injection the calcite in the vicinity of the wellbore is not entirely dissolved. The influence of calcite dissolution is reflected in the reservoir fluid pH (Figure 27): In the "direct brine scenario" the reservoir fluid pH in the vicinity of the wellbore remains close to pH=7.0, while in the "acidising scenario" it is close to pH=4.6 while the pH neutralisation front is pushed away up to 7m from the injection wellbore.

The model results supports the hypothesis that acidising upon drilling completion will assist in pushing the injected brine pH neutralisation front further away from the wellbore by removal of calcite in reservoir rock close to the injection well. However, there are some uncertainties due to the model not being able to account for the acid inhibition kinetics in the model. Hence, the true effect of optimizing silica polymerisation inhibition property cannot be tested.

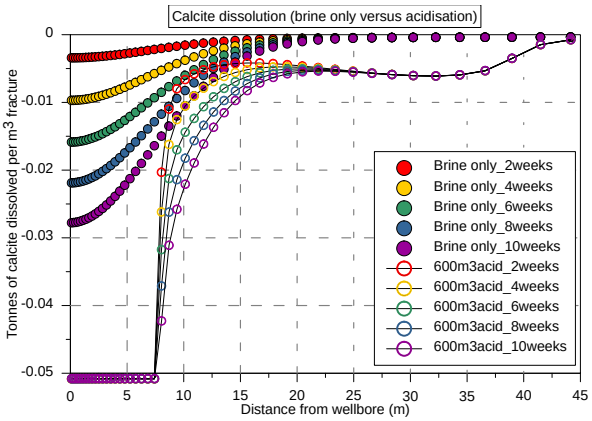

Figure 26: Calcite dissolution after acidising (referred to as "600m^3") compared with direct brine injection with no acidising upon completion of drilling (referred to as "Brine only").

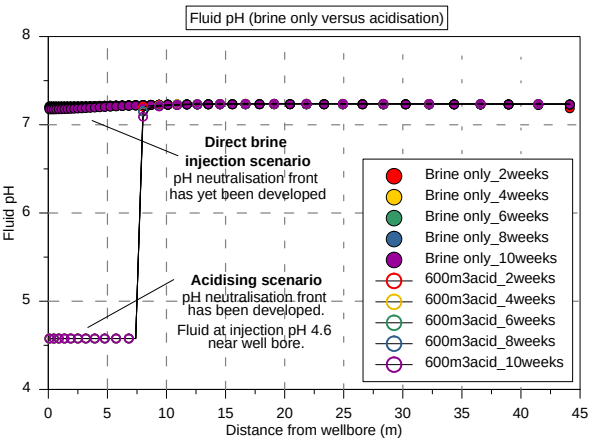

Figure 27: Fluid pH of brine injection after acidising (referred to as "600m^3") compared with direct brine injection with no acidising upon completion of drilling (referred to as "Brine only").

4. CONCLUSION

One-dimensional radial reactive transport models have been created for three injection wells to understand the different characteristics and behaviors in association to the injection fluid-reservoir rock interaction. Model matches between modelled and observed injectivity indices have been achieved choosing appropriate controlling parameters including initial specific reactive surface area of amorphous silica, various permeability laws, and fracture permeability where required.

The model results suggest that amorphous silica is the main contributor to the reduction in porosity and permeability, influencing the well performance. Delayed deposition resulting from inhibited polymerisation cannot be accounted for in the model. No anhydrite scaling is modelled. Model also suggests that reservoir fluid pH neutralisation in the vicinity of the injection well can be caused by two stages: during an early stage of operation, significant neutralisation results from calcite dissolution. The fast calcite dissolution kinetics leads to a sharp neutralisation front. At a later stage of operation, once calcite is completely dissolved, bulk rock acid dissolution involving minerals such as chlorite and epidote is initiated. Their quantity is about one order of magnitude less than calcite, and dissolution kinetics is slower, and results in a gradual neutralisation front further away from the wellbore.

From a modelling perspective, three main controlling factors that contribute towards the differing characteristics of injection wells are identified. Porosity-permeability relationship of the geologic media plays a role in controlling the extent of the permeability decline resulting from porosity reduction. Wells with larger feedzone thicknesses show a more intense and localized deposition near the wellbore; whereas wells with smaller feedzone thicknesses, show a less intense and more widespread deposition, as the injected fluid reaches further away from the wellbore to react with the same volume of reservoir rock. Higher injection flow rate introduce more aqueous silica available for amorphous silica deposition in the reservoir; however it enhances the calcite dissolution, subsequently pushing the neutralisation front further away from the wellbore. Given a robust acid inhibition system, “maximized injection load strategy” could be effective.

Based on this understanding of injection fluid-reservoir rock interactions, further simulations were conducted to identify opportunities in the reservoir injection management. As explained above, “maximized injection load strategy” could be effective with a robust acid inhibition system. Condensate-brine switching shows short-term benefits in reducing the amount of amorphous silica deposited, in contrast to brine only injection. Model results also supports the hypothesis of effective removal of calcite by acidising, which could potentially minimize the reservoir fluid pH neutralisation near the injection wellbore.

ACKNOWLEDGEMENTS

We would like to thank Mercury for the opportunity to publish this paper.

REFERENCES

Addison, S.J., Brown, K.L., von Hirtz, P.H., Gallup, D.L., Winick, J.A., Siega, F.L. and Gresham, T.J. (2015) Brine Silica Management at Mighty River Power, New Zealand. *Proceedings World Geothermal Congress.*

Bethke, C. (2011) Geochemical and Biogeochemical Reaction Modelling. Cambridge University Press.

Brown, K. (2011) Thermodynamics and kinetics of silica scaling. *Proceedings International Workshop on Mineral Scaling.*

Buscarlet, B. and Hernandez, D. (2014) Geochemical modelling of an injection well. *Proceedings 36th New Zealand Geothermal Workshop.*

Carrol, S., Mroczek, E., Alai, M. and Ebert, M. (1998) Amorphous silica precipitation (60 to 120ºC): Comparison of laboratory and field rates. *Geochemica et Cosmochimica Acta.* Vol.62, No.8, pp. 1379-1396.

Gallup, D. (1997) The interaction of silicic acid with sulfurous acid scale inhibitor *Geothermal Resources Council Transactions.* Vol. 21.

Grant, M. and Bixley, P. (2011) Geothermal Reservoir Engineering. Academic Press.

Iceland GeoSurvey (ISOR) (2013) The Iceland Water Chemistry Group. WATCH software, http://www.geothermal.is/software

Palandri, J.L. and Kharaka, Y.K. (2004) A compilation of rate parameters of water-mineral interaction kinetics for application to geochemical modelling, U.S. Geological Survey.

Verma, A. and Pruess, K. (1988) Thermohydrological conditions and silica redistribution near high-level nuclear wastes emplaced in saturated geological formations. *J. Geophys. Res.* Vol.93, pp. 1159-1173

Xu, T., Sonnenthal, E., Spycher, N. and Pruess K. (2006) TOUGHREACT – A simulation program for non-isothermal multiphase reactive geochemical transport in variably saturated geologic media: Applications to geothermal injectivity and CO_2 geological sequestration. *Computers & Geosciences.* Vol.32, pp. 145-165.

Xu, T., Sonnenthal, E., Spycher, N. and Pruess, K. (2012) TOUGHREACT User’s Guide: A Simulation Program for Non-isothermal Multiphase Reactive Geochemical Transport in Variably Saturated Porous Media. Lawrence Berkeley National Laboratory, Berkeley, California 94720.

Zeng Z., Seatres Jr. J. and Mroczek E. (2013) WATCH automator: an excel based data processor for multiple geochemical samples. *Proceedings New Zealand Geothermal Workshop.*